Jinkyu Yang
Graduate Aerospace Laboratories (GALCIT), California Institute of Technology, Pasadena, CA 91125; Mechanical Engineering Department, University of South Carolina, Columbia, SC 29208

Sophia N. Sangiorgio[1]
Department of Orthopedic Surgery, University of California, Los Angeles, J. Vernon Luck, MD Orthopedic Research Center Los Angeles Orthopedic Hospital, Los Angels, CA 90007
e-mail: Sophia.biomechanics@gmail.com

Sean L. Borkowski
J. Vernon Luck, MD Orthopaedic Research Center, Los Angeles Orthopedic Hospital, Los Angeles, CA 90007

Claudio Silvestro

Luigi De Nardo
Dipartimento di Chimica, Materiali e Ingegneria Chimica "G. Natta," Politecnico di Milano, Milano 20133, Italy

Chiara Daraio
Graduate Aerospace Laboratories (GALCIT), California Institute of Technology, Pasadena, CA 91125

Edward Ebramzadeh
Department of Orthopedic Surgery, University of California, Los Angeles, J. Vernon Luck, MD Orthopedic Research Center, Los Angeles Orthopaedic Hospital, Los Angeles, CA 90007

Site-Specific Quantification of Bone Quality Using Highly Nonlinear Solitary Waves

Osteoporosis is a well recognized problem affecting millions of individuals worldwide. The ability to diagnose problems in an effective, efficient, and affordable manner and identify individuals at risk is essential. Site-specific assessment of bone mechanical properties is necessary, not only in the process of fracture risk assessment, but may also be desirable for other applications, such as making intraoperative decisions during spine and joint replacement surgeries. The present study evaluates the use of a one-dimensional granular crystal sensor to measure the elastic properties of bone at selected locations via direct mechanical contact. The granular crystal is composed of a tightly packed chain of particles that interact according to the Hertzian contact law. Such chains represent one of the simplest systems to generate and propagate highly nonlinear acoustic signals in the form of compact solitary waves. First, we investigated the sensitivity of the sensor to known variations in bone density using a synthetic cancellous bone substitute, representing clinical bone quality ranging from healthy to osteoporotic. Once the relationship between the signal response and known bone properties was established, the sensor was used to assess the bone quality of ten human cadaveric specimens. The efficacy and accuracy of the sensor was then investigated by comparing the sensor measurements with the bone mineral density (BMD) obtained using dual-energy x-ray absorptiometry (DEXA). The results indicate that the proposed technique is capable of detecting differences in bone quality. The ability to measure site-specific properties without exposure to radiation has the potential to be further developed for clinical applications. [DOI: 10.1115/1.4007364]

Keywords: bone elasticity, solitary waves, nonlinear diagnostics, nondestructive evaluation (NDE)

1 Introduction

According to the National Institutes of Health Osteoporosis and Related Bone Diseases National Resource Center, more than $40 \times$ million Americans are at risk of fracture due to osteoporosis or low bone density. Osteoporosis can influence surgical decision making and clinical outcomes, particularly in hip and spine surgeries. As the 'baby boomer' generation ages and demands for a continued active and pain-free lifestyle increase, the incidence of joint replacement surgery also increases [1]. With the frequency of total joint and spine surgeries expected to increase over the next decades, the ability to perform accurate in vivo measurement of bone quality in the clinical setting would be beneficial [2–4].

Currently, the tools available for bone quality assessment include dual-energy x-ray absorptiometry (DEXA), which is the clinical gold-standard, along with quantitative computerized tomography (qCT) and quantitative ultrasound (QUS), which are more comprehensive. However, none offer comprehensive site-specific evaluation of bone mechanical properties in a noninvasive and time-efficient manner. Although DEXA scans are considered to be an effective tool to screen for osteoporosis and osteopenia, this is an oversimplification of a very complex mechanical phenomenon. Dual-energy x-ray absorptiometry is a two-dimensional

[1]Corresponding author.

Contributed by the Bioengineering Division of ASME for publication in the JOURNAL OF BIOMECHANICAL ENGINEERING. Manuscript received September 7, 2011; final manuscript received April 26, 2012; accepted manuscript posted August 17, 2012; published online October 1, 2012. Assoc. Editor: Sean S. Kohles.

quantification that averages the bone mineral density (BMD) over a large geometric area (not volume) of interest. Contrary to this simplification, bone is anisotropic and nonhomogeneous, and strength in any given direction is influenced not only by BMD, but also by the complex microstructural orientation of the organic collagen matrix in which the mineral portion is embedded. Therefore, the BMD, as determined by DEXA, is just one characteristic of a very complex structure.

Correlations of the BMD with the pull-out strength of various spine implants and fracture strength and risk have been reported [5,6]; however the results have been debated [7] and, due to the simplification of the areal BMD, a wide range of correlations have been found. Therefore, supplemental evaluation would be beneficial. Such an evaluation could have a strong impact on clinical decision making, both prior to and during surgeries. For example, many recent novel implants introduced for the treatment of degenerative disorders of the spine are contraindicated for patients with poor bone quality, as determined by DEXA. For example, one such device indicated for the treatment of lumbar spinal stenosis is contraindicated for patients with a T score < -2.5 [8]. However, this T score is based on an average density across the L1-L4 vertebrae, and may not represent the quality of individual posterior elements this device relies upon for fixation and mechanical support. Similarly, some studies have suggested that an anterior-posterior DEXA scan may overestimate the bone quality of the lumbar spine for devices which require vertebral body fixation, such as pedicle-based devices, due to the added cortical-rich regions in the posterior elements [9–13]. Since bone mineral density is just one aspect of the complex understanding of bone quality, a supplemental technique must be developed.

This study introduces and evaluates a novel method for the nondestructive site-specific evaluation of bone mechanical properties based on nonlinear acoustic pulses (i.e., highly nonlinear solitary waves, HNSWs). Highly nonlinear solitary waves are compact agglomerates of energy, which are generated by a balance of nonlinear and dispersive effects in intrinsically nonlinear media, such as granular and layered materials [14,15]. The fundamental understanding of the formation and propagation properties of HNSWs has allowed the development of several engineering applications, including shock and impact absorbing layers [16,17], acoustic lenses [18], and diagnostic scanning devices [19]. The use of HNSWs as information carriers in biomedical devices offers several advantages over conventional ultrasound-based technologies, such as QUS [20,21]. In principle, HNSWs can reach higher signal amplitudes compared to normal ultrasound signals [18]. This is expected to improve the overall signal-to-noise ratio and resolution of biomedical instruments; for example, in acoustic imaging. Furthermore, the propagation of HNSWs is highly sensitive to the mechanical properties of inspection media [22,23], which can enhance the accuracy and reliability of the mechanical wave-based diagnostic method for biomedical applications.

In the present study, we assembled a granular crystal to generate and propagate HNSWs for the site-specific evaluation of bone properties. To analyze the effects of the bone mechanical properties on the signal response, we employed a discrete particle numerical model [14,23] that combined the granular chain and bone structural properties to simulate the propagation and reflection of HNSWs. To validate the numerical model, we performed preliminary experimental HNSW tests on a range of artificial bone materials with known mechanical properties. Once the relationship between the signal response and the bone properties was established, we assessed the bone quality of human cadaveric femurs in highly localized bone regions. The bone quality assessment derived from the HNSW method was then compared to the bone density of the cadaveric specimens from the DEXA scans. Using these numerical and experimental approaches, we demonstrated the efficacy of the proposed HNSW-based evaluation method to detect the material properties of human cadaveric bone.

2 Materials and Method

2.1 HNSW-Based Evaluation Method

2.1.1 Experimental Setup. A one-dimensional granular crystal was assembled using 20 stainless steel beads (McMaster-Carr, Elmhurst, Illinois, type 440C, elastic modulus $E = 200$ GPa, density $\rho = 7780$ kg/m^3, Poisson's ratio $\nu = 0.27$, and radius $R = 9.525$ mm) (see Fig. 1). A granular crystal consists of a one-dimensional chain of tightly packed spheres that interact according to the Hertzian contact interaction law [19]. A mechanical impact on one end of the granular crystal has been shown to generate single or trains of HNSWs that propagate stably in the chain of particles [14]. Previous studies have shown that the scattering of these solitary waves at the interface between the granular chain and an elastic medium is affected by the mechanical properties of the material adjacent to the granular chain [22,23]. In this study, the HNSWs that propagate from the interface of the granular chain and adjacent bone were analyzed to investigate the bone material properties.

A single HNSW was generated by impacting the chain of beads with a striker particle, identical to the other particles in the chain. To control the striker impact, we used a DC-powered linear solenoid to release the striker from a drop height of 5 mm [23]. The temporal profiles of both the incident and reflected solitary waves traveling in the chain of particles were recorded using an instrumented bead containing a calibrated piezoceramic layer (TYPE-850, APC International, Mackeyville, PA) [16]. In this study, the instrumented bead was positioned at the 14th position from the interface (i.e., the 7th bead from the top of the chain, excluding the striker). The force histories measured by the instrumented particle were acquired using an NI data acquisition card (PCI-6115, National Instruments, Austin, Texas), which was connected to a computer for digital signal processing.

2.1.2 Numerical Setup. A discrete particle numerical model [14,23] was used to analyze the particle's dynamics in the granular crystal and the wave's interaction with the bone specimens. In this model, the particles in the monodispersed granular chain are described as lumped masses connected by nonlinear springs [14] (see Fig. 2). The forces between neighboring particles are regulated

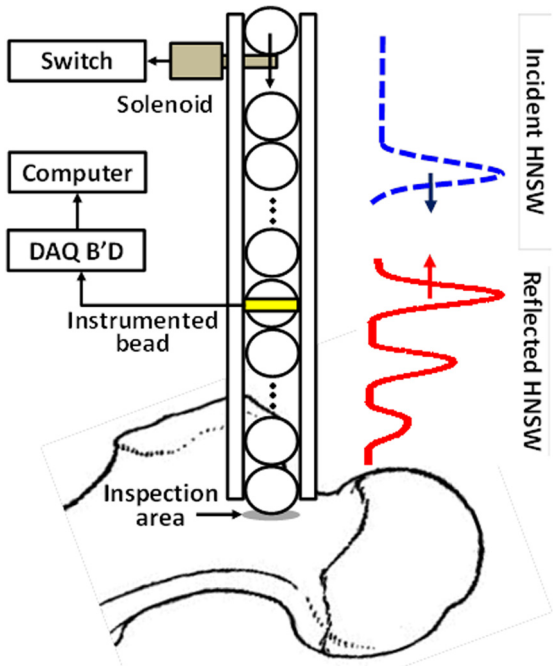

Fig. 1 Schematic diagram of a granular crystal-based sensor. The vertical chain is composed of 20 spherical particles constrained by guides. The incident (dashed) and reflected HNSWs (solid), triggered by the striker impact, are recorded by the instrumented bead.

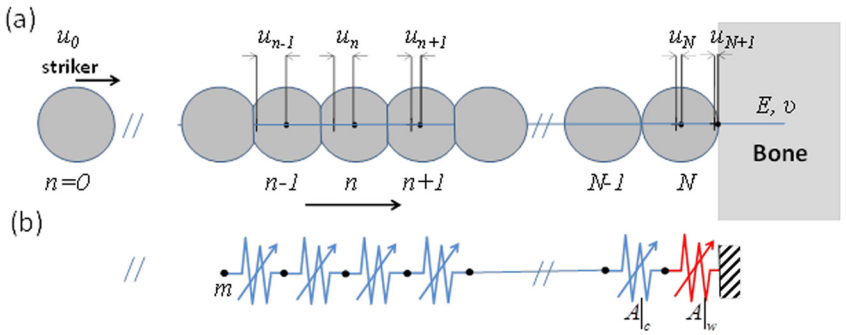

Fig. 2 (*a*) Schematic diagram showing the simplified model for the granular chain and bone contact. (*b*) The interaction of granular particles with the bounding bone can be modeled using a discrete particle model composed of point masses and nonlinear springs.

by the Hertzian contact law expressed as $F \propto \delta^{3/2}$, where F is the compressive force and δ is the displacement approach between particles [24]. The particle's equation of motion can be expressed as

$$m\ddot{u}_n = A_n[u_{n-1} - u_n]_+^{3/2} - A_{n+1}[u_n - u_{n+1}]_+^{3/2} + f, \quad n \in \{1, ..., N\},$$

$$A_n \equiv \begin{cases} A|_c = \dfrac{E\sqrt{2R}}{3(1-\nu^2)} & n \in \{1, ..., N\} \\ A|_w = \dfrac{4\sqrt{R}}{3}\left(\dfrac{1-\nu^2}{E} + \dfrac{1-\nu_w^2}{E_w}\right)^{-1} & n = N+1 \end{cases} \tag{1}$$

Here, m is the mass of the bead, u_n is the displacement of the given particle from its equilibrium position, and f is the body force applied to the bead (i.e., gravity, in this study). The granular crystal was composed of a total number of $N = 20$ beads, with the particle $n = 0$ representing the striker bead having a defined initial velocity. The bracket $[s]_+$ takes only positive values and returns to 0 if $s < 0$. This means that the discrete particle model for the tightly-packed granular chain is dictated by the double nonlinearity: a nonlinear force under compression and a zero tensile force [25]. The coefficient of the nonlinear spring in the chain $A|_c$ is a function of the elastic modulus (E), Poisson's ratio (ν), and the radius of the particles (R). The nonlinear spring coefficient $A|_w$ at the end of the chain is governed by the material properties of the bone denoted by the subscript w, as well as the bead material properties.

Ordinary differential solvers in MATLAB® [26] were used to numerically integrate Eq. (1) and model the formation and propagation of a single HNSW upon the striker impact (see the blue curve in Fig. 1). The model also captures the propagation of the reflected pulses, which are generated after the incident HNSW interacts with the bone material (see the red curve in Fig. 1).

We studied the variation of the reflected HNSWs as a function of the different bone material properties. Specifically, we investigated the relationship between the time of flight (TOF) of HNSWs and the bone's effective stiffness parameter (ESP), which represents the local stiffness of the anisotropic and nonhomogeneous bone structure at specific locations. In this study we defined the impulse's TOF as the time elapsed between the arrival of the incident solitary wave on the instrumented sensor particle in the chain and the arrival of the reflected solitary wave after interacting with the bone. For the analysis, we considered only the arrival of the first reflection (herein referred to as the primary reflected solitary wave) and neglected the formation of secondary pulses. This is because the secondary reflected solitary waves are affected not only by the localized mechanical properties of the bone specimens, but also by their boundary conditions.

It is notable that the discrete particle model, as expressed in Eq. (1), is dictated by the elastic modulus of the bone material, not by the density. In other words, the behavior of HNSWs is governed by the mechanical stiffness of the bone, not by the BMD. Therefore, this proposed HNSW-based method performs a direct assessment of one bone mechanical property, which may be useful as a supplement to BMD measurement by DEXA for a better measure of overall bone quality. By numerically solving the equation of the particle's motion, we acquired the relationship between the TOF and the ESP of bone material. Given the experimentally measured TOF values, we used this numerical relationship to back-calculate the corresponding ESP, i.e., the effective stiffness of bone specimens at specific locations.

2.1.3 Validation Using Synthetic Bone With Known Material Properties. We first performed experimental and numerical investigations on the responsiveness of the HNSWs to the mechanical properties of neighboring media, using artificial bone materials with clinically relevant material properties. The primary focus was twofold: (1) evaluating the sensitivity of the proposed HNSW-based method, and (2) validating our numerical scheme based on the discrete particle model. The investigation was performed using seven different samples of rigid polyurethane foam (Pacific Research Laboratories, Inc., Vashon, Washington) to simulate clinical bone quality ranging from healthy to severely osteoporotic (see Table 1). These polyurethane specimens are designed, tested, and marketed specifically to be compliant with ASTM F-1839-08 "Standard Specification for Rigid Polyurethane Foam

Table 1 Specifications of artificial cancellous bone samples made of polyurethane foam

Sample	Density (g/cc)	Compressive strength (MPa)	Stiffness modulus (MPa)	Osteoporotic categorization
1	0.08	1.0	32	High risk of fracture
2	0.16	2.2	58	Osteoporotic
3	0.24	4.9	123	Healthy
4	0.32	8.4	210	Healthy
5	0.48	18	445	Healthy
6	0.64	31	759	Healthy
7	0.80	48	1148	Healthy

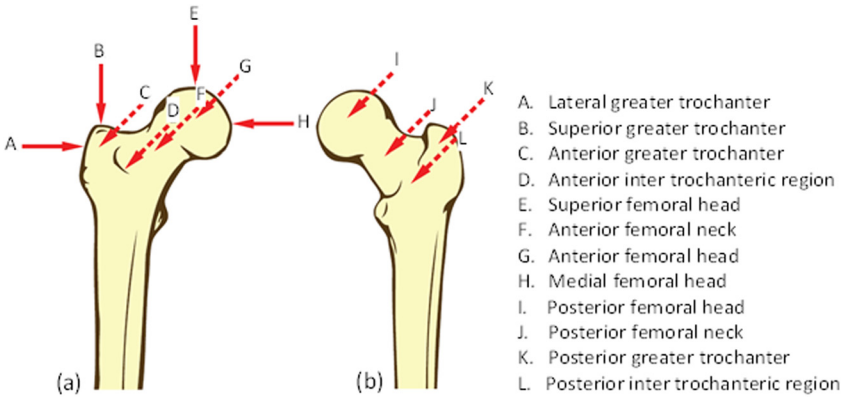

Fig. 3 Schematic diagram of a human femur with 12 measurement locations for the HNSW-based evaluation in (*a*) anterior and (*b*) posterior views

for Use as a Standard Material for Testing Orthopaedic Devices and Instruments," and therefore, manufacturing techniques are highly reproducible. Each artificial cancellous bone sample was cut into a $50 \times 50 \times 50$ mm block and five measurements of reflected HNSWs were obtained for each sample. The experimental data were analyzed in relation to the known properties of the synthetic foam and were then compared to the numerical results obtained from the discrete particle model.

2.2 Evaluation of Proximal Femoral Bone Quality

2.2.1 Specimen Preparation. Ten fresh-frozen human cadaveric femurs were selected to represent a range of bone quality and sizes. High-resolution anteroposterior and mediolateral radiographs were taken of each specimen using an HP Faxitron Series™ x-ray system (438O5N, Hewlett Packard Company, Palo Alto, California) at the standard 15% clinical magnification. Radiographic analysis of each specimen was performed prior to experimentation to determine bone health. Additionally, the radiographs were examined for signs of evident bone disease, injury, or abnormalities. Excess soft tissue was carefully removed in the proximal region of the femur to expose the cortical surface of each specimen. Care was taken during dissection to preserve the natural surface of the bone. All specimens were kept frozen before and after testing and thawed to room temperature immediately prior to HNSW evaluation.

2.2.2 DEXA Analysis. The bone mineral density (BMD) of all ten specimens was assessed by dual-energy x-ray absorptiometry (DEXA) using a Hologic 2000 bone densitometer (Hologic, Inc., Waltham, MA) and a soft tissue substitute, in order to mimic patient conditions. For each specimen, the standard clinical regions were measured: (1) femoral neck, (2) trochanteric region, (3) inter trochanteric region, (4) Ward's area, and (5) proximal femur. For each scan, area (cm^2), bone mineral content (g), and areal BMD (g/cm^2) were assessed.

2.2.3 Direct HNSW Measurements of Cadaveric Femurs. Using the same apparatus that was used to measure the synthetic bone specimens, site-specific nondestructive evaluation was conducted for each cadaveric femur. For each specimen, the HNSW-based evaluation was performed at 12 locations: anterior femoral neck, posterior femoral neck, superior greater trochanter, lateral greater trochanter, anterior greater trochanter, posterior greater trochanter, anterior inter trochanteric region, posterior inter trochanteric region, superior femoral head, medial femoral head, anterior femoral head, and posterior femoral head (see Fig. 3). For each location, five repetitive tests were performed to acquire the mean time of flight (TOF) of the primary reflected solitary waves. Based on the numerical relationship between the TOF and ESP developed by the discrete particle model, the local stiffness at different locations of the proximal femur was calculated using the experimentally measured mean time of flight (TOF).

2.3 Statistical Analysis. The categorical input variables for this study were: (1) the BMD measurement areas (five scanning areas of DEXA testing), and (2) the HNSW recording location (twelve testing locations of site-specific HNSW-based evaluation). The primary outcome variables were: (1) the BMD, and (2) the ESP. A statistical analysis was performed to determine the strength of the correlation between the BMD measurements and the HNSW measurements. The SPSS 15.0 statistical analysis software (SPSS, Inc., Chicago, IL) was used to assess the bivariate Pearson correlation between: (1) the proximal femur BMD (non-site-specific) and the ESP, and (2) site-specific BMD and ESP. Pearson correlation (r) values were determined, each with an associated p-value. Linear regression analysis was used to determine the strength of each correlation, represented by the slope of each regression.

3 Results

3.1 Preliminary Validation Using Synthetic Bone Material. Figure 4 reports the experimental and numerical results obtained from the interaction of HNSWs with synthetic bone. The dotted

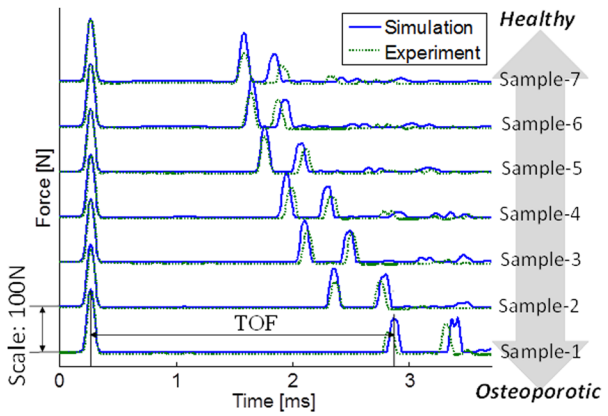

Fig. 4 Solitary wave interaction with artificial bone samples. The blue (solid) lines denote numerical force profiles, while the green (dotted) lines represent experimental measurements. To ease visualization, the signals are shifted by 100 N in the vertical axis. A group of rigid polyurethane foam simulates clinical bone quality ranging from healthy to osteoporotic status. The time of flight (TOF) values are extracted from the raw signals by measuring the time elapsed between the incident and the first reflected waves, measured by the instrumented particle.

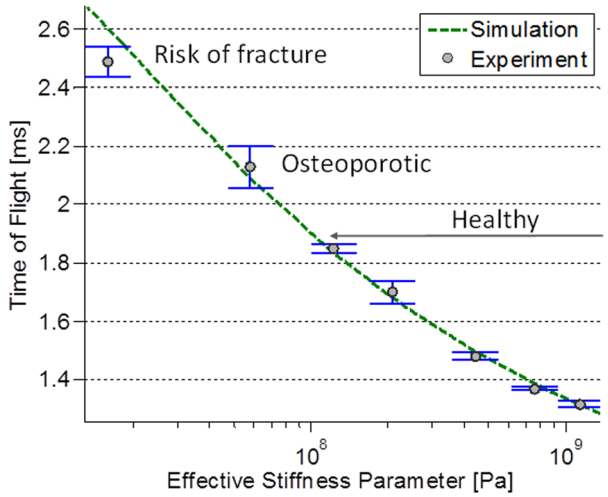

Fig. 5 Time of flight (TOF) values as a function of the ESP stiffness parameters. The blue line denotes the numerical results based on the discrete particle model, while the circles represent the experimental results. The error bars are standard deviation values obtained from five experimental measurements using artificial bone specimens. The "high risk of fracture" or "osteoporotic" samples generate larger TOF values in comparison to the "healthy" specimens.

curves represent the experimental signals recorded by the instrumented particle in the granular chain, while the solid lines denote the numerical results derived from the discrete particle model, as described in Section 2. For the derivation of the numerical results, we employed the synthetic bone properties provided by the manufacturer (see Table 1). The signals obtained from the different bone materials are shifted vertically to ease visual comparison. The first impulse evident in the plots corresponds to the arrival of the incident solitary wave on the 7th bead in the chain (identical for all tests). The subsequent impulses represent the arrival of reflected solitary waves after the incoming impulse interacted with the polyurethane foam specimens. We observe a dramatic difference in the time of arrival of the reflected waves by comparing the results obtained from the different foam samples. In particular, the HNSW interaction with the more "osteoporotic" specimens results in longer delays in the arrival of the reflected solitary waves to the instrumented sensor than that of the "healthier" specimens.

The dependence of the TOF on the synthetic bone's ESP is shown in Fig. 5, both experimentally and numerically. Note that in this synthetic bone testing, the effective stiffness parameters in the abscissa are essentially the nominal elastic moduli of the rigid polyurethane samples due to the homogeneous and isotropic nature of the specimens. It is evident that the TOF of the primary solitary waves exhibit a strong dependence on the ESP of the synthetic bone. According to the experimental results, the TOF in the "osteoporotic" sample (2.13 ms; Sample 2 in Fig. 4) is increased by 61.4% in comparison to the healthiest sample (1.32 ms; Sample 7). A further delay in the arrival time of the primary reflected solitary waves is obtained if the bone quality is degraded to the "high risk of fracture" level (2.49 ms; Sample 1).

In Figs. 4 and 5, we found that the numerical results closely reproduce the strong correlation between the TOF and the ESP. In other words, the numerical simulations of the granular crystal's interaction with the bone material are capable of accurately predicting the formation and propagation of solitary waves reflected from the bone interface. Based on these numerical results, we established a relationship between the TOF and the ESP. Using the least square fitting of the numerical data, the TOF (in seconds) can be mathematically expressed as a function of the ESP (in Pascal)

$$\begin{aligned} &\mathrm{TOF} = a \cdot \mathrm{ESP}^b + c \\ &a = 0.0331 \pm 0.0088 \\ &b = -0.1514 \pm 0.0228 \\ &c = -1.016 \times 10^{-4} \pm 0.313 \times 10^{-4} \end{aligned} \tag{2}$$

The coefficients are shown with their 95% confidence interval. This numerical relationship, based on the discrete particle model, enables us to derive the ESP of bone specimens, given the measured TOF values via the proposed granular crystal sensor.

3.2 Cadaveric Bone Testing. Following radiographic analysis, one specimen had to be excluded from further analysis due to the presence of a large tumor in the proximal femur. Therefore, a total of nine specimens were used for analysis. The analysis was focused on the proximal femur, femoral neck, greater trochanter, and inter trochanteric region.

3.2.1 BMD Results. The specimens represented a wide range of bone quality, with the proximal femur BMD measurements

Table 2 BMD measurements via DEXA

Statistic	Proximal femur BMD (g/cm^2)	Femoral neck BMD (g/cm^2)	Trochanter BMD (g/cm^2)	Inter trochanteric BMD (g/cm^2)
Mean	0.73	0.60	0.52	0.87
Std. Dev.	0.19	0.17	0.16	0.23
Median	0.68	0.51	0.47	0.85
Min.	0.41	0.37	0.29	0.47
Max.	1.08	0.86	0.80	1.31

Table 3 Effective stiffness parameter (ESP) measurements via the HNSW-based method

Femoral region	Location	Mean (GPa)	Std. Dev. (GPa)	Median (GPa)	Min. (GPa)	Max. (GPa)
Neck	Anterior	0.90	0.54	0.94	0.25	1.75
	Posterior	1.90	0.57	1.91	1.15	2.70
Greater trochanter	Axial	1.10	0.84	1.29	0.05	2.55
	Lateral	0.78	0.54	0.80	0.17	1.85
	Anterior	0.60	0.47	0.73	0.06	1.34
	Posterior	0.36	0.32	0.28	0.06	1.12
Inter	Anterior	2.20	0.98	2.08	0.94	3.92
	Posterior	0.54	0.51	0.47	0.01	1.69
Head	Axial	0.27	0.10	0.28	0.12	0.43
	Lateral	0.16	0.08	0.13	0.09	0.32
	Anterior	0.22	0.09	0.21	0.11	0.33
	Posterior	0.22	0.05	0.20	0.17	0.31

Table 4 Correlations of ESP versus BMD

		Non site-specific			Site-specific		
Femoral region	HNSW location	Pearson correlation	*p*-value	Slope	Pearson correlation	*p*-value	Slope
Neck	Anterior	0.46	0.217	1.28	0.50	0.168	1.64
	Posterior	0.85	0.004	2.53	0.88	0.002	3.04
Greater trochanter	Axial	0.78	0.013	3.42	0.77	0.016	4.12
	Lateral	0.66	0.055	1.85	0.76	0.017	2.65
	Anterior	0.91	0.001	2.21	0.91	0.001	2.73
	Posterior	0.86	0.003	1.42	0.86	0.003	1.75
Inter trochanter	Anterior	0.91	0.001	4.61	0.89	0.001	3.75
	Posterior	0.69	0.040	1.83	0.69	0.038	1.52

ranging from 0.41 g/cm^2 to 1.08 g/cm^2. The largest BMD measurements were found in the inter trochanteric region, while the smallest were found in the greater trochanter (see Table 2).

3.2.2 ESP Results. The ESP values calculated locally using HNSWs varied depending on the femoral region, as well as on the HNSW evaluation location (see Table 3). On average, the highest ESP was found in the posterior femoral neck and the anterior inter trochanteric region, with mean ESP values of 1.90 GPa and 2.20 GPa, respectively. The smallest range of values was found in the femoral head, with mean ESP values of 0.16 GPa to 0.27 GPa.

3.2.3 BMD versus ESP. Non-site-specific correlations were calculated by correlating the ESP of a specific region, as measured by the HNSW testing, with the proximal femur BMD, as measured by DEXA (see Table 4). The largest non-site-specific correlation was found at the anterior greater trochanter and at the anterior inter trochanteric region, both with Pearson correlation values of $r = 0.91$ and $p = 0.001$. Figs. 6(*a*)–6(*c*) show the correlation between the proximal femur BMD and the ESP measured, respectively, from the femoral neck, the greater trochanter, and the inter trochanteric region.

Site-specific correlations were calculated by correlating the ESP of a specific region in the HNSW testing with the BMD in the corresponding region of the DEXA testing. The largest site-specific correlation was $r = 0.91$ and $p = 0.001$, found for the correlation of the anterior greater trochanter ESP with the greater trochanter BMD. The smallest correlations were found for the anterior femoral neck and the anterior inter trochanteric locations (see Table 4). The site-specific correlations between the BMD and the ESP are reported in Figs. 6(*d*)–6(*f*) for the femoral neck, greater trochanter, and inter trochanteric regions.

4 Discussion

The HNSW has the potential of providing useful information for the evaluation of bone quality via the direct contact with bone, particularly, local bone stiffness represented by the effective stiffness parameter (ESP). The reflected HNSWs are formed by the mechanical interaction of the last particle in the granular crystal sensor and the surface of the bone at the contact point (18,40). The particles' rebound motion is governed by the local stiffness of the bone structure. This rebound mechanism, controlled by highly localized elastic interactions at the contact point, is the key difference between our measurement and other techniques based on ultrasonic waves. In contrast, conventional techniques can only provide average information over a large bone area through the "pitch-catch" or "impact-echo" scheme [27].

In this study, the interaction of HNSWs with bone specimens was simulated using a discrete particle model that combines the response of the granular chain and of the bone structure. Based on the wave dynamics in the vicinity of the sensor and bone interface, this numerical model enabled us to establish the relationship between the TOF and the ESP of the bone. The efficacy and precision of this model was experimentally validated by testing synthetic blocks modeled after cancellous bone of varying mechanical properties, representing a range of bone densities. The time of flight varied on the order of milliseconds between the strongest, most dense synthetic testing block and the weakest, least dense sample. This is in contrast to the order-of-microseconds delays obtained with ultrasonic wave measurements for the conventional QUS [21]. This "slower" signal propagation for the HNSWs could potentially translate into a higher reliability, sensitivity, and effectiveness of the HNSW-based diagnostics, but has yet to be established. Further studies are needed.

Following the testing of our numerical model, an in vitro study of human cadaveric femurs allowed the ESP in highly localized bone regions using the HNSW-based testing. Based on the statistical analysis, the ESP measurements were correlated with both the site-specific bone mineral density (BMD) and the non-site-specific BMD, that is, the BMD at the femoral neck, for example, which is often clinically used. This demonstrates the potential capability of the HNSW method to both evaluate the effective stiffness of localized bone regions ans detect differences in bone density. Additionally, the slopes of the regression lines in the femoral neck and greater trochanter of site-specific correlations, which are two regions prone to injury, were greater than those of the regression lines for non site-specific correlations.

The mechanical stiffness of cadaveric femurs, in terms of the elastic modulus, has been broadly studied in the literature. For cortical bone, wide ranges of elastic modulus have been reported, with values as low as 0.69 GPa along the femoral shaft [28], to values greater than 20 GPa [29–32]. Similarly, trabecular bone also shows a wide range of elastic properties, with elastic modulus values varying from 0.49 GPa to almost 10 GPa [32]. A more recent study of cortical bone biopsies from osteoarthritic patients showed an elastic modulus range of 0.69 GPa to 3.37 GPa [28]. The values of the effective stiffness parameters measured in our study also show a wide range, between 0.01 and 3.92 GPa, but tend to be in the lower range of the elastic modulus reported in earlier literature [32]. It is important to mention that the proposed evaluation method obtains the localized bone stiffness information in the vicinity of the sensor/bone interface that embraces both the surface of the bone (cortical shell) and the inner (cancellous) material. This suggests that the calculated ESP values in this study are through-thickness properties of bone specimens at selected locations. In addition, it is well known that changes in the bone's material properties can occur in different regions of the bone itself and depend on other confounding factors such as age, gender, bone density, and testing conditions [33–38]. Therefore, it is difficult to make direct comparisons between the ESP values reported in this study to the elastic moduli reported in the literature.

Clearly, a supplemental site-specific measurement, based on a mechanical measurement, as opposed to bone mineral content, would be beneficial for a more specific assessment of bone quality, since BMD is only one piece of a very complex puzzle that is bone quality. In this study, site-specific correlations between the

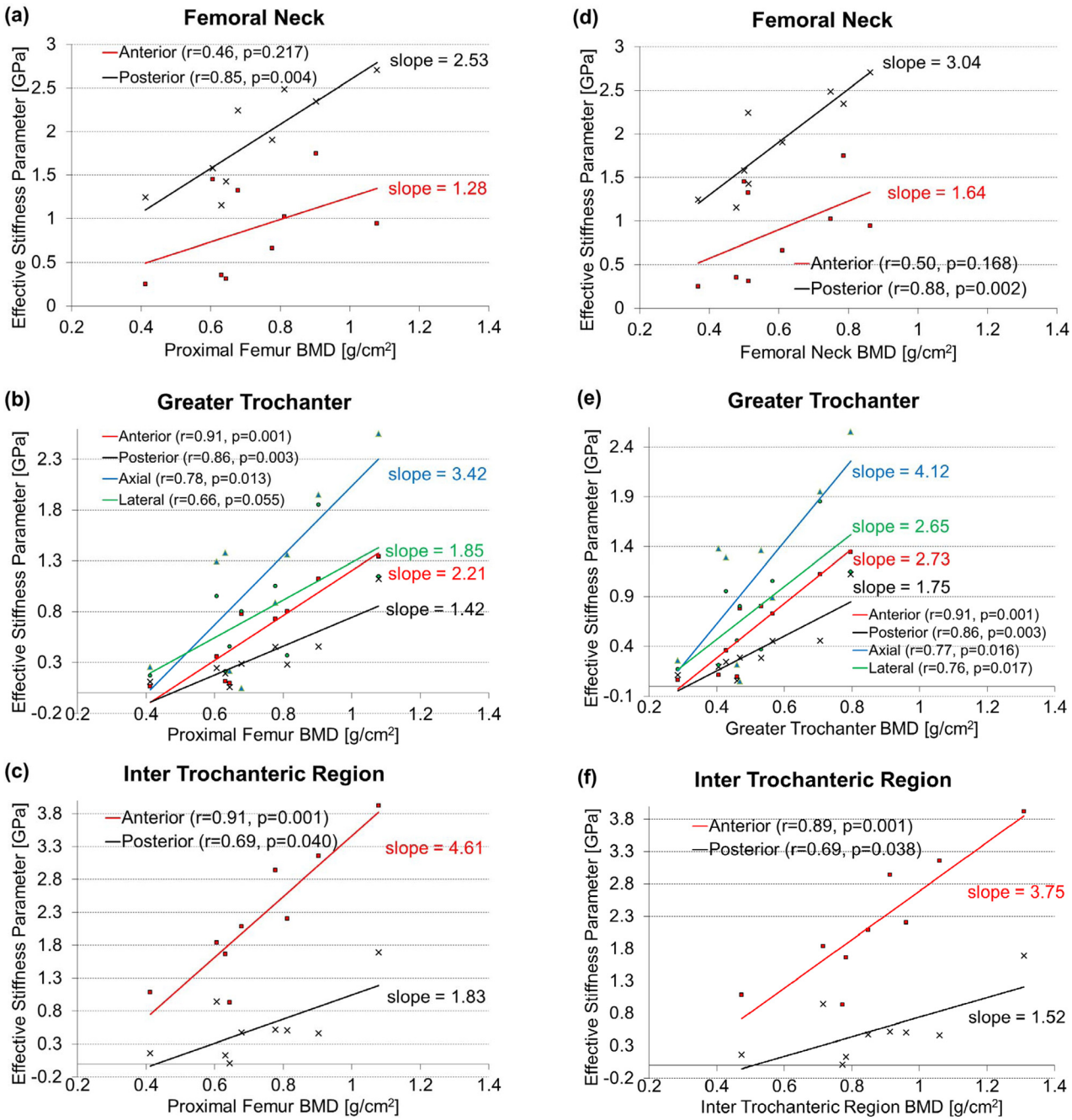

Fig. 6 Correlations for the ESP versus BMD. (*a*) Non site-specific, femoral neck ESP versus proximal femur BMD. (*b*) Non site-specific, greater trochanter ESP versus proximal femur BMD. (*c*) Non site-specific, inter trochanteric ESP versus proximal femur BMD. (*d*) Site-specific, femoral neck ESP versus femoral neck BMD. (*e*) Site-specific, greater trochanter ESP versus greater trochanter BMD. (*f*) Site-specific, inter trochanteric ESP versus inter trochanteric BMD.

ESP and BMD (measured by DEXA) were found in the femoral neck, greater trochanter, and inter trochanteric regions. The Pearson correlation values obtained from the measurements were found to be as high as $r = 0.91$ and $p = 0.001$. However, low correlations were also found in some regional measurements, such as at the anterior femoral neck (when compared to the femoral neck BMD), with a correlation of $r = 0.50$. This regional difference could simply be a result of the areal scanning technique employed by DEXA. For example, the BMD measurements may have been more heavily influenced by the posterior region, and thus, the calculated ESP in the posterior femoral neck location correlates better with the femoral neck BMD than the ESP in the anterior region. Additionally, the range of correlations could be due to the nonuniformity of bone tissues, such as anisotropic differences and cortical thinning.

In evaluating the results, both the slope of each regression line and the associated p-value were considered. The slope of the line indicated the magnitude of the effect, while the p-value indicated the certainty associated with that relationship. While the statistical significance for the correlations found that comparing the site-specific and non-site-specific measurements (proximal femur BMD) to the HNSW measurements were comparable, the slopes of the site-specific regression lines were larger. These higher slopes for the site-specific correlations suggested that the HNSW-based evaluation of bone quality is more sensitive in specific regions; hence, the greater change in magnitude for the same

change in the BMD, when correlated with specific region bone density measurements.

This study establishes the foundation for utilizing highly nonlinear solitary waves in the nondestructive site-specific evaluation of bone's mechanical properties. The results indicate the proposed evaluation method based on HNSWs is capable of extracting localized bone stiffness measurements for different regions and locations in the proximal femur, thereby providing a compact, quick, and sensitive site-specific measurement of the bone quality. The proposed HNSW-based method could potentially supplement conventional methods of determining bone quality and could prove to be useful for in vivo measurement of bone mechanical properties in the clinical setting.

This study had limitations which need to be addressed in future studies. For example, there was no independent direct measurement of bone mechanical properties, such as by mechanical testing of the specimens. Furthermore, the findings with the novel method were compared to DEXA which, as discussed, has many limitations due to the nature of the areal BMD measurement. In future studies, qCT measurements should be performed, which are directly comparable to the site-specific measurement locations by the HNSW sensor. Despite these limitations, the present study represents a necessary first step toward the development of this method: a novel technique to assess bone mechanical properties when direct access to the cortical surface is available, such as during surgery.

Acknowledgment

The authors are very grateful to Ashleen Knutsen and Sachith Dunatunga for their assistance in preparing specimens and performing tests. They also thank Jeremy Kalma for his assistance in the preparation of figure illustrations and experiments. C.D. acknowledges support from the National Science Foundation, Grant Nos. CMMI-825345 and CMMI-844540 (CAREER).

References

[1] Crowninshield, R. D., Rosenberg, A. G., and Sporer, S. M., 2006, "Changing Demographics of Patients With Total Joint Replacement," Clin. Orthop. Relat. Res., **443**, pp. 266–272.
[2] Kurtz, S. M., Ong, K. L., Schmier, J., Mowat, F., Saleh, K., Dybvik, E., Karrholm, J., Garellick, G., Havelin, L. I., Furnes, O., Malchau, H., and Lau, E., 2007, "Future Clinical and Economic Impact of Revision Total Hip and Knee Arthroplasty," J. Bone Joint Surg. Am., **89**(3), pp. 144–151.
[3] Kurtz, S. M., Lau, E., Ong, K., Zhao, K., Kelly, M., and Bozic, K. J., 2009, "Future Young Patient Demand for Primary and Revision Joint Replacement: National Projections From 2010 to 2030," Clin. Orthop. Relat. Res., **467**, pp. 2606–2612.
[4] Deyo, R. A., and Mirza, S. K., 2006, "Trends and Variations in the Use of Spine Surgery," Clin. Orthop. Relat. Res., **443**, pp. 139–146.
[5] Lochmuller, E. M., Muller, R., Kuhn, V., Lill, C. A., and Eckstein, F., 2003, "Can Novel Clinical Densitometric Techniques Replace or Improve DXA in Predicting Bone Strength in Osteoporosis at the Hip and Other Skeletal Sites?," J. Bone Miner. Res., **18**, pp. 906–912.
[6] Myers, E. R., Hecker, A. T., Rooks, D. S., Hipp, J. A., and Hayes, W. C., 1993, "Geometric Variables From DXA of the Radius Predict Forearm Fracture Load In Vitro," Calcif. Tissue Int., **52**, pp. 199–204.
[7] Kanis, J. A., 2002, "Diagnosis of Osteoporosis and Assessment of Fracture Risk," Lancet, **359**, pp. 1929–1936.
[8] Zucherman, J. F., Hsu, K. Y., Hartjen, C. A., Mehalic, T. F., Implicito, D. A., Martin, M. J., Johnson, D. R. II, Skidmore, G. A., Vessa, P. P., Dwyer, J. W., Puccio, S. T., Cauthen, J. C., and Ozuna, R. M., 2005, "A Multicenter, Prospective, Randomized Trial Evaluating the X STOP Interspinous Process Decompression System for the Treatment of Neurogenic Intermittent Claudication: Two-Year Follow-Up Results," Spine, **30**, pp. 1351–1358.
[9] Zmuda, J. M., Cauley, J. A., Glynn, N. W., and Finkelstein, J. S., 2000, "Posterior-Anterior and Lateral Dual-Energy X-Ray Absorptiometry for the Assessment of Vertebral Osteoporosis and Bone Loss Among Older Men," J. Bone Miner. Res., **15**, pp. 1417–1424.
[10] Yu, W., Gluer, C. C., Grampp, S., Jergas, M., Fuerst, T., Wu, C. Y., Lu, Y., Fan, B., and Genant, H. K., 1995, "Spinal Bone Mineral Assessment in Postmenopausal Women: A Comparison Between Dual X-Ray Absorptiometry and Quantitative Computed Tomography," Osteoporosis Int., **5**, pp. 433–439.
[11] Bjarnason, K., Hassager, C., Svendsen, O. L., Stang, H., and Christiansen, C., 1996, "Anteroposterior and Lateral Spinal DXA for the Assessment of Vertebral Body Strength: Comparison With Hip and Forearm Measurement," Osteoporosis Int., **6**, pp. 37–42.
[12] Cheng, X. G., Nicholson, P. H., Boonen, S., Lowet, G., Brys, P., Aerssens, J., Van der Perre, G., and Dequeker, J., 1997, "Prediction of Vertebral Strength In Vitro by Spinal Bone Densitometry and Calcaneal Ultrasound," J. Bone Miner. Res., **12**, pp. 1721–1728.
[13] Myers, B. S., Arbogast, K. B., Lobaugh, B., Harper, K. D., Richardson, W. J., and Drezner, M. K., 1994, "Improved Assessment of Lumbar Vertebral Body Strength Using Supine Lateral Dual-Energy X-Ray Absorptiometry," J. Bone Miner. Res., **9**, pp. 687–693.
[14] Nesterenko, V. F., 2001, *Dynamics of Heterogeneous Materials*, Springer-Verlag, New York.
[15] Idler, C., Zucherman, J. F., Yerby, S., Hsu, K. Y., Hannibal, M., and Kondrashov, D., 2008, "A Novel Technique of Intra-Spinous Process Injection of PMMA to Augment the Strength of an Inter-Spinous Process Device Such as the X STOP," Spine, **33**, pp. 452–456.
[16] Daraio, C., Nesterenko, V. F., Herbold, E. B., and Jin, S., 2006, "Energy Trapping and Shock Disintegration in a Composite Granular Medium," Phys. Rev. Lett., **96**, p. 058002.
[17] Hong, J., 2005, "Universal Power-Law Decay of the Impulse Energy in Granular Protectors," Phys. Rev. Lett., **94**, p. 108001.
[18] Spadoni, A., and Daraio, C., 2010, "Generation and Control of Sound Bullets With a Nonlinear Acoustic Lens," Proc. Natl. Acad. Sci. U.S.A., **107**, 7230–7234.
[19] Khatri, D., Daraio, C., and Rizzo, P., 2009, "Coupling of Highly Nonlinear Waves With Linear Elastic Media," Proc. SPIE, **6934**, p. 72920.
[20] Gluer, C. C., Wu, C. Y., and Genant, H. K., 1993, "Broadband Ultrasound Attenuation Signals Depend on Trabecular Orientation: An In Vitro Study," Osteoporosis Int., **3**, pp. 185–191.
[21] Baroncelli, G. I., Battini, R., Bertelloni, S., Brunori, E., de Terlizzi, F., Vierucci, F., Cipriani, P., Cioni, G., and Saggese, G., 2010, "Analysis of Quantitative Ultrasound Graphic Trace and Derived Variables Assessed at Proximal Phalanges of the Hand in Healthy Subjects and in Patients With Cerebral Palsy or Juvenile Idiopathic Arthritis: A Pilot Study," Bone, **46**, pp. 182–189.
[22] Job, S., Melo, F., Sokolow, A., and Sen, S., 2005, "How Hertzian Solitary Waves Interact With Boundaries in a 1D Granular Medium," Phys. Rev. Lett., **94**, p. 178002.
[23] Yang, J., Silvestro, C., Khatri, D., De Nardo, L., and Daraio, C., 2010, "Interaction of Highly Nonlinear Solitary Waves With Linear Elastic Media," Phys. Rev. E, **83**, p. 046606.
[24] Johnson, K. L., 1985, *Contact Mechanics*, Cambridge University Press, New York.
[25] Nesterenko, V. F., Daraio, C., Herbold, E. B., and Jin, S., 2005, "Anomalous Wave Reflection at the Interface of Two Strongly Nonlinear Granular Media," Phys. Rev. Lett., **95**, p. 158702.
[26] Shampine, L. F., and Reichelt, M. W., 1997, "The MATLAB ODE Suite," SIAM J. Sci. Comput., **18**, pp. 1–22.
[27] Njeh, C. F., Boivin, C. M., and Langton, C. M., 1997, "The role of Ultrasound in the Assessment of Osteoporosis: A Review," Osteoporosis Int., **7**, pp. 7–22.
[28] Wachter, N. J., Krischak, G. D., Mentzel, M., Sarkar, M. R., Ebinger, T., Kinzl, L., Claes, L., and Augat, P., 2002, "Correlation of Bone Mineral Density With Strength and Microstructural Parameters of Cortical Bone In Vitro," Bone **31**, pp. 90–95.
[29] Rho, J. Y., Ashman, R. B., and Turner, C. H., 1993, "Young's Modulus of Trabecular and Cortical Bone Material: Ultrasonic and Microtensile Measurements," J. Biomech., **26**, pp. 111–119.
[30] Wirtz, D. C., Schiffers, N., Pandorf, T., Radermacher, K., Weichert, D., and Forst, R., 2000, "Critical Evaluation of Known Bone Material Properties to Realize Anisotropic FE-Simulation of the Proximal Femur," J. Biomech., **33**, pp. 1325–1330.
[31] Keller, T. S., Mao, Z., and Spengler, D. M., 1990, "Young's Modulus, Bending Strength, and Tissue Physical Properties of Human Compact Bone," J. Orthop. Res., **8**, pp. 592–603.
[32] Goldstein, S. A., 1987, "The Mechanical Properties of Trabecular Bone: Dependence on Anatomic Location and Function," J. Biomech., **20**, pp. 1055–1061.
[33] Augat, P., Link, T., Lang, T. F., Lin, J. C., Majumdar, S., and Genant, H. K., 1998, "Anisotropy of the Elastic Modulus of Trabecular Bone Specimens From Different Anatomical Locations," Med. Eng. Phys., **20**, pp. 124–131.
[34] Reilly, D. T., and Burstein, A. H., 1974, "Review Article. The Mechanical Properties of Cortical Bone," J. Bone Joint Surg. Am., **56**, pp. 1001–1022.
[35] Crofts, R. D., Boyce, T. M., and Bloebaum, R. D., 1994, "Aging Changes in Osteon Mineralization in the Human Femoral Neck," Bone, **15**, pp. 147–152.
[36] Bell, K. L., Loveridge, N., Power, J., Garrahan, N., Meggitt, B. F., and Reeve, J., 1999, "Regional Differences in Cortical Porosity in the Fractured Femoral Neck," Bone, **24**, pp. 57–64.
[37] Majumdar, S., Kothari, M., Augat, P., Newitt, D. C., Link, T. M., Lin, J. C., Lang, T., Lu, Y., and Genant, H. K., 1998, "High-Resolution Magnetic Resonance Imaging: Three-Dimensional Trabecular Bone Architecture and Biomechanical Properties," Bone, **22**, pp. 445–454.
[38] Snyder, S. M., and Schneider, E., 1991, "Estimation of Mechanical Properties of Cortical Bone by Computed Tomography," J. Orthop. Res., **9**, pp. 422–431.